periodica polytechnica

Mechanical Engineering
55/1 (2011) 3–14
doi: 10.3311/pp.me.2011-1.01
web: http://www.pp.bme.hu/me
© Periodica Polytechnica 2011

RESEARCH ARTICLE

Mechanical behavior of glass fiber-reinforced bosses: experiments and FE simulations

Enikő Soós / *Tibor* Goda

Received 2011-04-30

Abstract

This paper, on the one, reports experimental data on injection molded polyamide 6 boss reinforced with 30 wt% of short glass fibers (PA6 GF30), on the other, presents an FE modelling technique for modeling viscoplastic material response. Before the tests all the specimens were conditioned to a moisture content of 1 wt%. The water concentration in the material was checked by weighting. All the mechanical tests have been carried out in compression mode (compression test, compression loading-unloading test, cyclic compression loading-unloading test, compression loading-relaxation-unloading-recovery test) by using a Zwick 1454 type tensile tester equipped with a temperature controlled chamber. The fiber orientation and the strain distribution in the boss was investigated by scanning electron microscopy (SEM) and optical grating technique. The modeling technique presented is based on the overlay method and the generalized Maxwell model. In order to take plastic deformations into consideration the linear viscoelastic Maxwell-model was generalized to viscoplasticity by replacing the linear spring with an "elastic-plastic" spring. The applicability of the model was proved by finite element simulation.

Keywords

short glass fiber-reinforced polyamide · linear viscoelasticity · viscoplasticity · compression test · finite element analysis

Enikő Soós
Department of Machine and Product Design, BME, H-1111, Műegyetem rkp. 3. Budapest, Hungary
e-mail: soos.eniko@gt3.bme.hu

Tibor Goda
Department of Machine and Product Design, BME, H-1111, Műegyetem rkp. 3. Budapest, Hungary
e-mail: goda.tibor@gt3.bme.hu

1 Introduction

Thread-cutting screws are widely used in different engineering applications to fasten assemblies together by means of the boss (see Fig. 1) and screw. In this economical form of fastening the threads of the boss are cut by a thread-cutting screw during the insertion process. In the last 10 years, engineers focused their attention to the optimization of the screw/boss design and the insertion process. One of the main conclusions was that the optimized screw and boss designs are material specific. Due to this it is extremly important to characterize material behavior properly. In most cases, the base material for the boss is polycarbonate (PC), acrylonitrile butadiene styrene (ABS), polypropylene (PP) or polyamide (PA). In order to improve the mechanical behavior of the boss material, in many cases, short fiber-reinforcement is used as it is the case at PA6 GF30, where short glass fibers (GF) are used to reinforce the thermoplastic, semicrystalline polyamide 6 (PA6).

In [1], stress-strain tests (tensile tests at different strain rates) and dynamic mechanical analysis (DMA) were used to study the viscoelastic material behavior of PA6 GF30 (Akulon, from DSM, the Netherlands). The tensile tests were carried out in a temperature range of 23-75°C, while, in case of tensile mode DMA tests, the specimens were studied during heating from −20 to 100°C at a heating rate of 4°C/min. In the latter case the stress values were sufficiently small thus the mechanical response of the specimens was within the linear viscoelastic range. The specimens were injection moulded and conditioned at 23°C and 50% RH (relative humidity) for two weeks before testing. One of the most important conclusions was that the temperature dependence of the shift factors used at the construction of the master curve – can be well described by the WLF (Williams-Landel-Ferry) equation. At a reference temperature of 45°C, the C_1 and C_2 parameters of the WLF equation were 20.9 and 120°C, respectively.

Stan et al [2] studied the viscoelastic properties of short glass fibre-reinforced polyamide 66 (PA66 GF30) by DMA and indentation tests. In the latter case, the viscoelastic behaviour can be characterized by the response of the material to constant load. The DMA tests were performed by using a cantilever beam con-

figuration and a wide temperature range (from -30 to 200°C at a heating rate of 4°C/min). At the construction of storage modulus master curve ($T_{ref} = 60$°C) the temperature dependency of shift factor was described by the WLF equation. In order to improve the accuracy different WLF constants were used above and below the glass transition temperature ($T_g \approx 60$°C). The WLF constants were as follows: (a) $C_1 = 69.52$, $C_2 = 537.3$°C if $T > T_{ref}$; (b) $C_1 = 93.78$, $C_2 = 503$°C if $T < T_{ref}$. Despite the great difference of WLF constants the temperature dependency of the shift factor is very similar (see later) in [1] and [2].

[3] and [4] deal with the experimental study of glass fibre-reinforced polyamide 66 (DuPont™ Zytel® 70G35 HSLX) specimens at room temperature. All mechanical tests were carried out with a stress or strain controlled tensile load at two different humidity states, dry-as-solded (DAM) or conditioned at the equilibrium with an air containing 50% of relative humidity (RH50). The material was tested in tension at stress rates ranging over four decades and in cyclic tension with loading histories combining creep, stress relaxation or strain recovery steps at different strain/stress levels. An important finding was that, under the measurement conditions of [3] and [4], residual strains appear above a stress threshold of 50-60 MPa only.

In this paper, the compressive behavior of short glass fibre-reinforced polyamide (PA6 GF30) is studied experimentally and numerically. As a first step various mechanical tests are performed on injection molded bosses having a certain moisture content. Then the parameters of linear viscoelastic 40–term generalized Maxwell-model are determined from a fit to storage modulus master curve. Finally, the generalization of the spring-dashpot model to viscoplasticity is made by replacing the linear spring with an "elastic-plastic" spring. The generalized material model is incorporated into an axi-symmetric FE model by using the overlay method.

2 Materials and methods

The mechanical tests were carried out of bosses made of polyamide 6 containing 30 wt% of short glass fibers produced by BASF (Ultramid® B3EG6). The bosses were injection moulded, their shape and dimensions are shown in Fig. 1. Before the tests the expanding end of the bosses (see below part of the boss in (Fig. 1a) was cut away and the bosses were drilled through by a drill of 6 mm. Due to this the specimens used in mechanical tests were hollow cylinders (Fig. 1b). Using the real boss as specimen is especially useful because, in this case, the fiber orientation and the shape of the real boss and the specimen are the same. Before testing the specimens were conditioned to a moisture content of 1 wt% which was checked by weighing. The conditioning was carried out according to [7].

Firstly the fiber orientation was investigated by scanning electron microscope (SEM), then mechanical tests, such as compression test, compression loading-unloading test, cyclic compression loading-unloading test, compression loading-relaxation-unloading-recovery test, were carried out at room or elevated

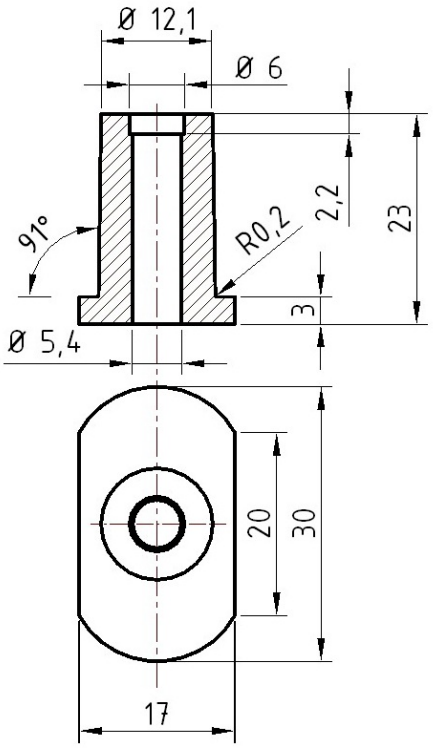

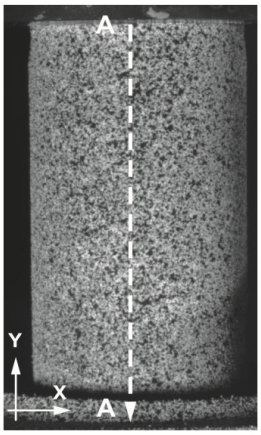

Fig. 1. PA6 GF30 boss (a) and specimen (b) (dimensions are in [mm]

temperature. In all the measurements performed at room temperature an extensometer was attached to the specimens using adequate clamping clips. The recorded force-displacement values were converted into engineering stress-strain curves. Besides the extensometer, the optical grating techniqe was also used to measure the strain field developed in the specimen (see Fig. 2). For this purpose the Aramis system of GOM was used. A short review of the optical grating technique can be found in [5]. Fig. 1b and Fig. 2 show the encoded surface of the specimen.

At elevated temperatures ($T = 40, 60$ and 80°C) only compression tests were carried out. In these cases, it was not possible to use the extensometer thus the axial strain was measured

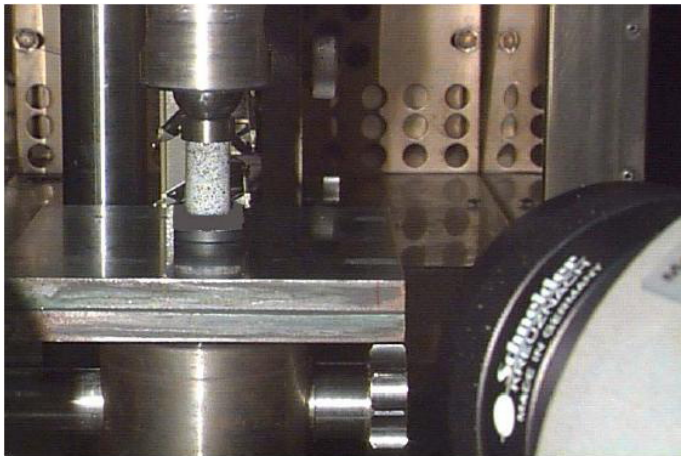

Fig. 2. Compression test (the strain field is measured by optical grating technique.

by optical grating technique only. All the tests presented above were performed on a Zwick 1454 type tensile tester with a test velocity (cross-head speed) of 0.8 mm/min. All the measurements were performed in displacement controlled mode. The effect of the friction force on the measured results and the degree of the barrelling were reduced by contaminating both the upper and below contact surfaces of the specimens with graphite powder before the tests.

All the mechanical tests presented were performed in the laboratory of tha Department of Mechanicel and Process Engineering at University of Kaiserslautern. The SEM photos were made in the laboratory of Institute of Composite Materials at University of Kaiserslautern.

3 Experimental results

3.1 Characterization of fiber orientation by electron microscope observations

Fiber orientation or more precisely the differences in fiber orientation of injection molded bosses has been characterised by observing polished cross-sections by scanning electron microscope (SEM). Glass fiber oriented a certain angle with respect to the cutting plane appears as ellipse on the SEM photo. Analysis of an ellipse allows the orientation of the fiber to be reconstructed. The measurement of the major and minor axes of the ellipses leads to the orientation angles of the glass fibers. At this point it must be mentioned that as signs of orientation angles can not be determined from the ellipses this approach may lead to inaccurate results. In the present case, each polished cross-section of the boss exhibited a skin-core morphology with different glass fiber orientations in the core and in the skin. In the skin the fibers are oriented parallel to the loading direction (axial direction) while, in the core, they are oriented normal to the longitudinal axis (see Fig. 3, Fig. 4).

3.2 Mechanical tests

Only a few papers are available in the literature which deal with the mechanical behavior of injection molded PA6 GF30.

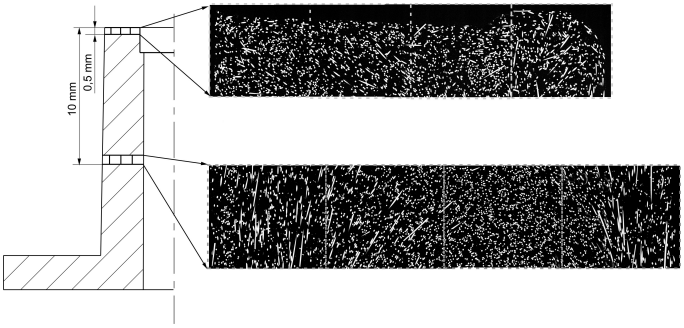

Fig. 3. Polished cross-sections of tha PA6 GF30 boss. Cutting plane is parallel to the longitudinal axis of boss.

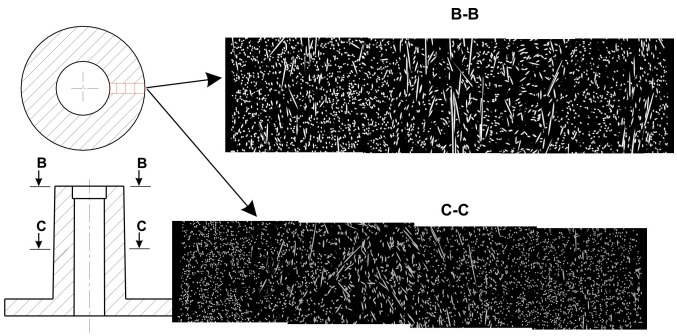

Fig. 4. Polished cross-sections at the top and in the middle of the PA6 GF30 boss. Cutting plane is normal to the longitudinal axis of boss.

Additionally, these papers usually study experimental behavior under uniaxial tension only. However, in many cases, the characteristic load of the boss is compression. This is why one important aim of the present paper is to report experimental data on injection molded PA6 GF30 subjected to compression. In order to avoid misunderstanding it must be mentioned that at the illustration of measures stress-strain diagrams the compressive stress and strain are assumed to have positive signs.

3.2.1 Compression tests and compression loading-unloading tests at room and elevated temperatures

The engineering stress-strain responses for two compression loading-unloading tests (M1 and M2) are shown in Fig. 5. The specimens were loaded at constant cross-head speed until the compressive force reached the value of 8.5 kN, after which they were unloaded at the same constant cross-head speed down to the zero stress. The maximum strain at the end of loading is about 7%, while the maximum stress is somewhat larger than 90 MPa. At the end of unloading i.e. at zero stress the strain is about 2%. As PA6 GF30 exhibits viscous effects (time-dependent behavior) the strain measured at the instant when the axial stress becomes zero decays with time (strain recovery). The strain recovery will be studied later at the loading-relaxation-unloading-recovery test. As it is well known, if the recovery of the initial configuration is only partial then one portion of the total deformation will be residual deformation. According to the physics of polymers the residual deformation may be viscous or plastic. In the former case, the viscous deformation comes into being at any stress level but its magnitude

varies with increasing stress. On the contrary, the plastic deformation does not come into being below the yield strength of the material. In the current study, authors, based on the findings of [3] and [4], assumed that the residual deformation of PA6 GF30 is due to plastic deformation. In respect of Fig. 5 it can be concluded that both the loading and unloading paths of the stress-strain diagram are non-linear and the transition from the nearly linear region to non-linear region is continuous i.e. there are no humps in the stress-strain diagram. As expected the curved (non-linear) loading and unloading paths form a hysteresis loop. The engineering stress-strain values depicted in Fig. 5 were computed from forces measured by the tensile tester and displacements measured by the extensometer.

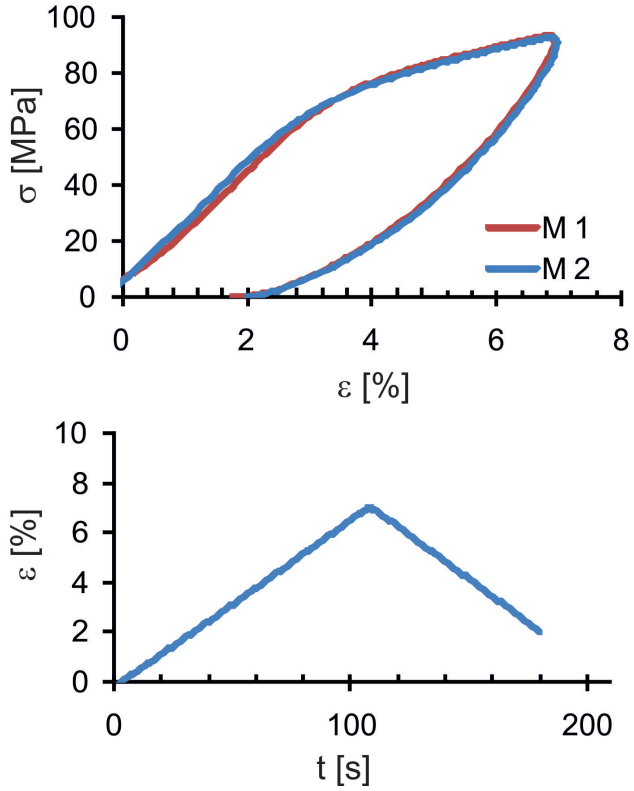

Fig. 5. (a) Axial engineering stress-strain (σ-ε) curves and (b) strain-time curve for compression loading-unloading test performed at room temperature (F_{max} = 8.5 kN, v (cross-head speed)= 0.8 mm/min). Strains were computed from displacements measured by extensometer, while engineering stresses were computed from force values measured by the tensile tester.

Similar engineering stress-strain curves can be seen in Fig. 6. However, theme stress-strain curves differ slightly from those seen in Fig. 5 because the strain values were measured - in depth of 2, 4, 6 and 8 mm from the top of the specimen (see line A-A in Fig. 1) –by optical grating technique. Consequently the optical grating technique allows local stress-strain curves to be constructed from strain values measured locally. According to this stress-strain curves depicted in Fig. 6 represent the local material behavior and shows clearly the inhomogenity of the boss.

Characteristic axial strain distributions measured by optical grating technique are shown in Fig. 7. The curves represent the strain distribution along line A-A. The strain distribution mea-

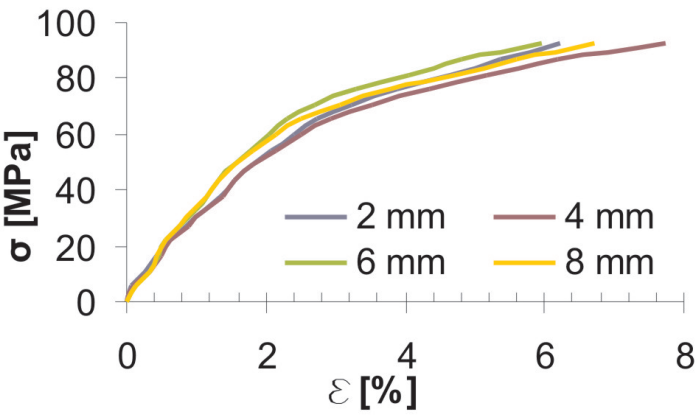

Fig. 6. Axial engineering stress-strain ($\sigma - \varepsilon$) curves for compression test performed at room temperature (F_{max} = 8.5 kN, υ = 0.8 mm/min). Strains were measured by optical garting technique in depth of 2, 4, 6 and 8 mm from the top of the specimen.

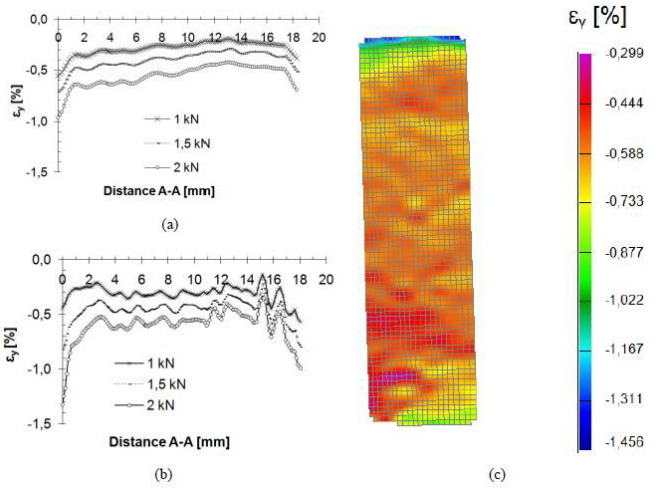

Fig. 7. Variation of ε_y strain component along line A-A at the end of loading in case of two different measurement (a) and (b) and the ε_y strain distribution at 2 kN compressive force (c).

sured at a compressive force of 2 kN is shown in Fig. 7. Disregarding the ends of the specimen the strains, at all load levels, decrease slightly as the distance A-A increases. This linear tendency can be explained by the conical form of the boss (The loaded cross section increases with increasing distance A-A.) It can also be seen that the strain at a load of 2 kN is about twice as large as the one at 1 kN.

Fig. 8 shows the engineering stress-strain response from uniaxial compression tests at temperature of 40, 60, and 80°C. The tests were carried out by constant cross-head speed of υ = 0.8 mm/min. The strains were measured by optical grating technique while the stress values were computed from the forces measured by the tensile tester. Fig. 8a and Fig. 8b show the local stress-strain diagrams measured in a depth of 4 and 12 mm from top of the specimen at different temperatures. As seen the response of the material is clearly shown to be dependent on the temperature. Increasing the temperature the material becomes less stiff. In all the cases, the loading path of the stress-strain

diagram is non-linear.

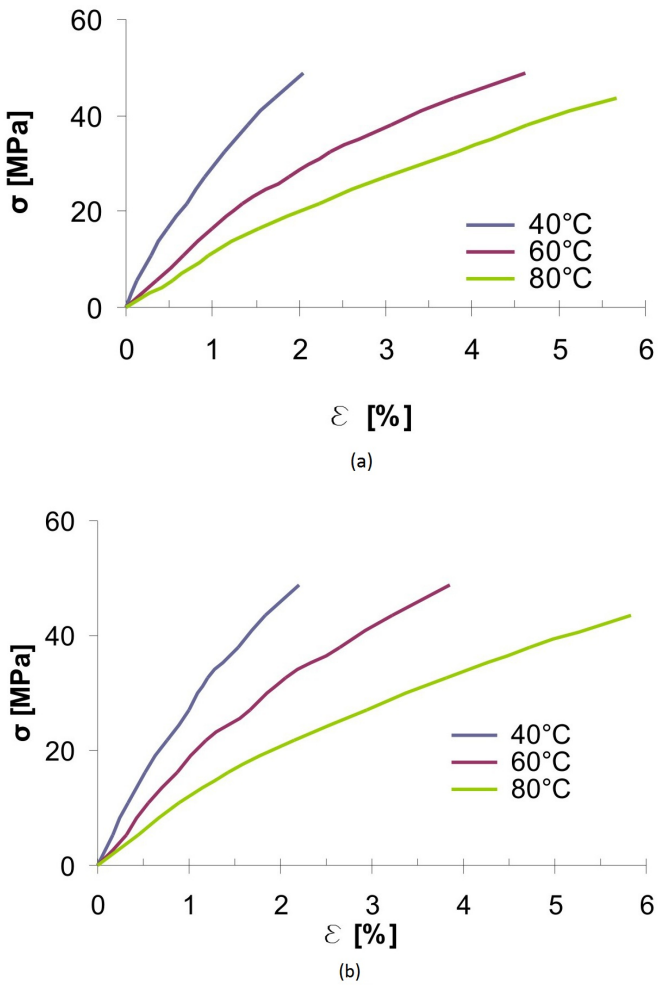

Fig. 8. Axial engineering stress-strain ($\sigma - \varepsilon$) curves for compression test performed at 40, 60 and 80°C ($F_{max} = 4.5$ kN, $v = 0.8$ mm/min). Strains were measured by optical grating technique in depth of 4 (a) and 12 mm (b) from the top of the specimen.

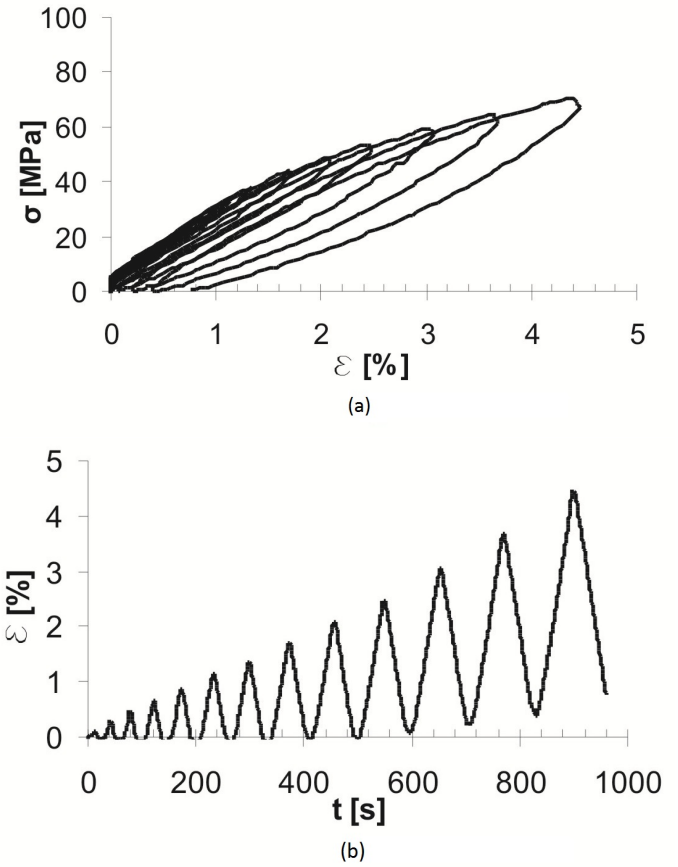

Fig. 9. Axial engineering stress-strain ($\sigma - \varepsilon$) curves and (b) strain-time curve for cyclic compression test performed at room temperature. The compressive force was increased by 0.5 kN at each new cycle until it reached 6.5 kN ($v = 0.8$ mm/min at both loading and unloading). Strains were computed from displacements measures by extensometer, while engineering stresses were computed from force values measured by the tensile tester.

3.2.2 Cyclic compression loading-unloading tests at room temperature

Three series of cyclic compression loading-unloading tests have been performed at room temperarure. Specimens were loaded with a constant cross-head speed of 0.8 mm/min up to the maximal compressive force 0.5 kN and unloaded with the same cross-head speed down to the zero stress. Then the specimen was reloaded (without holding the specimen at zero stress for a certain time period) with the same cross-head speed up to a force 0.5 kN grater than in the previous cycle. This loading-unloading process was continued until the maximal compressive force reached a value of 6.5 kN. At the highest clamping load the duration of the loading-unloading cycle was 120 s. As seen the strain at the end of unloading i.e. at zero stress becomes larger and larger as the load increases (see Fig. 9). It can also be concluded that the strain is totally recovered at low stresses. However at higher stresses the strain recovery is only partial.

The strain distributions along line A-A at the end of the loading phases (Fig. 10a) and at the instant when the axial stress becomes zero i.e. at the end of unloading phases (Fig. 10b) in each cycle are shown in Fig. 10a and Fig. 10b. Both diagrams show the results of five, subsequent cycles where the maximal compressive force was 0.5, 1, 1.5, 2 and 2.5 kN. Results belonging to the same cycle are representes by the same color. As Fig. 10 shows majority (about 90%) of strains disappears during uploading at each load level. At the same time the strain at the end of unloading can not be regarded as permanent (irreversible) strain beause PA6 GF30 exhibits delayed elastic deformation (The delayed elastic portion of the strain will be recovered at zero stress).

3.2.3 Compression loading-relaxation-uploading-recovery (LRUR) test

In the compression loading-relaxation-unloading-recovery (LRUR) test, specimens were compressed with constant cross-head speed to 2 kN clamping load (corresponds to a compressive stress of 22 MPa) where the position of the cross-head of the tensile tester was held constant for 16 h. As seen in Fig. 11a the stress decays exponentially in the relaxation phase. The relaxation test showed that during 16 h the compressive stress reduces

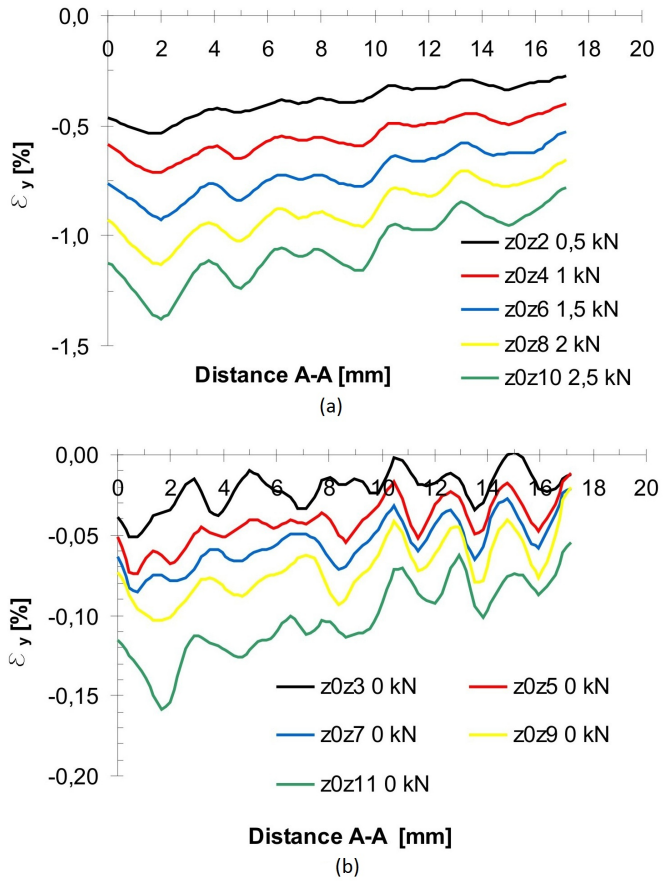

Fig. 10. Variation of ε_y strain component along the line A-A at the and of loading (a) and unloading (b) phases of a cyclic compression loading-unloading test performed at room temperature. Results belonging to the same cycle are represented be the same color. ($v = 0.8$ mm/min, $F = 0.5, 1, 1.5, 2$ and 2.5 kN)

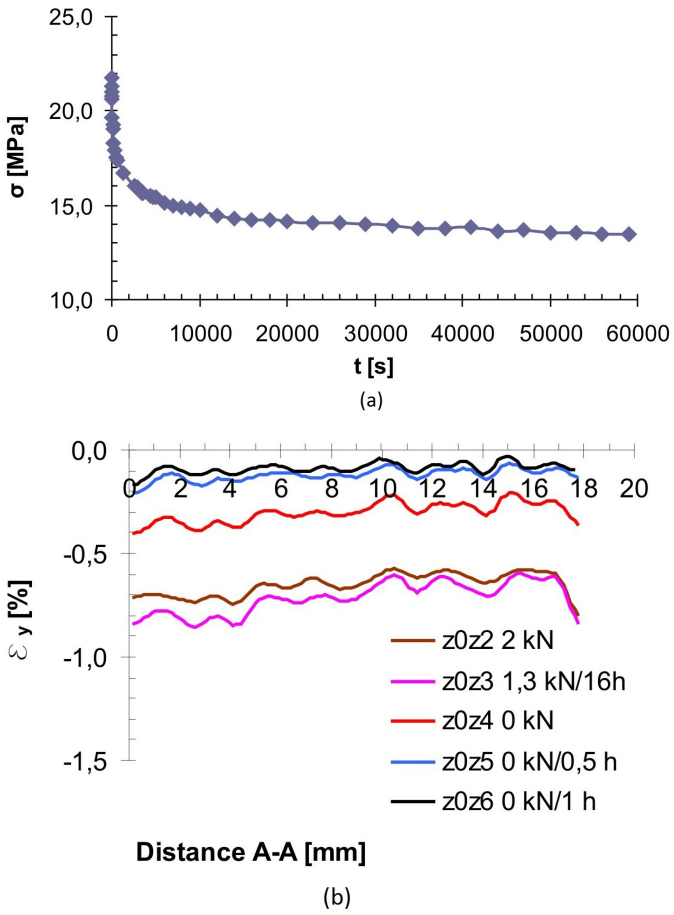

Fig. 11. (a) Stress decay during the relaxation phase and (b) strain distributions (along line A-A) at different time instants of the LRUR test ($T = 25°$C, $v = 0.8$ mm/min

with 39% (The stress decayed from 22 MPa to 13.5 MPa). At the end of holding period the specimens were unloaded to zero stress level. After unloading there was a strain recovery phase which was also investigated. The strain distribution along line A-A was measured at different time instants (at the end of loading, relaxation, unloading phase and at a recovery time of 0.5 and 1 h by the optical grating technique. Fig. 11b shows the strain distribution at different time instants. As it can be seen there is an intensive strain recovery after unloading. Majority of strains observed at the end of unloading phase recovered during 0.5 h. At the same time the recovery was not complete after 0.5 h because the strain decreased further for the following 30 min, resulting in a long-term recovery process. Nevertheless even a recovery time of 1 h was not long enough to recover the initial configuration. Similar to [3] and [4] it is difficult to decide whether ihe remaining strain is permanent or the time period for the recovery phase was not long enough to obtain a complete recovery (long-term reversible viscoelasticity). As it is well known viscoelastic deformations are reversible and disappear immediately or some time after unloading. Based on Fig. 11b it can be concluded that considerable plastic strain can not be observed under a compressive stress of 22 MPa.

4 Modelling

The increase in using thread-cutting screw joints for different applications leads to a strong need for the development of constitutive models dedicated to the simulation of the behavior during the operation phase. In order to model the material behavior of Ultramid we need a material model which is able to handle not only the viscoelastic but also the viscoplastic deformations. The details of such a material model are presented in this chapter. For simplicity, the inhomogeneous and anisotropic nature of PA6 GF30 are ignored i.e. the material is assumed to be homogemeous and isotropic.

4.1 Dynamic mechanical analysis

In order to study the viscoelastic response at low strains, among others, the dynamic mechanical analysis (DMA) is used, where the specimen undergoes repeated small-amplitude strains at different temperatures and excitation frequencies. As the authors had no chance to perform DMA measurement on Ultramid the temperature dependent storage modulus curve of Campus databank [8] was used for simulation purposes. In respect of PA6 GF30 (Ultramid, BASF) [8] consists of experimental data for both dry and conditioned specimens (see Fig. 12). The dry and conditioned state correspond to a moisture content of 0.2 and 2 wt% respectively. As the moisture content of the spec-

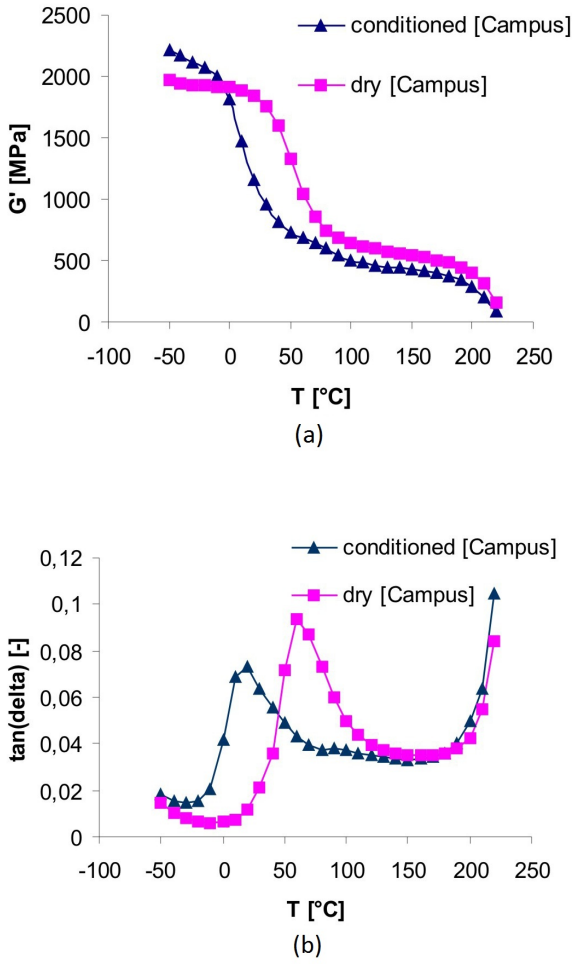

Fig. 12. Storage (shear) modulus vs. temperature (a) and loss factor vs. temperature (m) curves of PA6 GF30 (Ultramid, BASF) for dry and conditioned state [8]($f = 1$ Hz)

imens used in this study is between these two values we can assume that the material behavior is also somewhere between the ones corresponding to these conditioning states. This is the reason why authors use both measured characteristics (denoted as dry and conditioned) in the FE simulations. Glass transition temperature (T_g) of the dry and the conditioned PA6 GF30 (Ultramid, BASF) is about 60 and 20°C, respectively [8]. This shows clearly that the moisture content has a strong effect on the glass transition temperature.

Unfortunatelly, [8] does not contain additional temperature dependent storage modulus curves for frequencies other than 1 Hz hence it was not possible to construct the storage modulus master curves (storage modulus vs. frequency curve) of Ultramid. If the storage modulus master curves was available the parameters of a proper viscoelastic material model would be determined from a fit to the master curve.To overcome the difficulty caused by the incomplete DMA results of [8] authors made a literature review. This review proved that the temperature dependence of glass fiber-reinforced polyamids can be well described by the Williams-Landel-Ferry (WLF) equation. The WLF equation can be written as

$$\log a_T = \frac{-C_1(T - T_r)}{C_2 + (T - T_r)} \tag{1}$$

where a_T is the shift factor, T_r is the reference temperature, while C_1 and C_2 are the WLF parameters at the reference temperature T_r. Mano and Viana [1]found that, in case of PA6 GF30, the C_1 and C_2 parameter, of a reference temperature of 45°C, are 20.9 and 120°C. Unportunatelly, [8] contains neither the whole storage modulus master curve nor the WLF parameters of Ultramid. It is interesting to note that the WLF parameters of PA66 GF30 [2], at first sight, differ significantly from those of PA6 GF30 but, in fact, the temperature dependency of shift factors is very similar. In [2], it was found that the agreement with the measurement can be improved if two different sets of WLF parameters are used above and below the glass transition temperature ($T_r = T_g = 60$°C). The parameters obtained by this approach were as follows: (a) if $T > T_r$ then $C_1 = 69.52$, $C_2 = 537.3$°C; (b) if $T < T_r$ then $C_1 = 93.78$, $C_2 = 503$°C. The WLF parameters of [1] and [2] are difficult to compare because they belong to different reference temperature. However, as it is well known (see [9]), the WLF parameters at any reference temperature T_r (C_1 and C_2) may be easily related with those at T_g (C_{1g} and C_{2g}) by

$$C_1 = \frac{-C_{1g} \times C_{2g}}{C_{2g} + (T_1 - T_g)} \tag{2}$$

$$C_2 = -C_{2g} + (T_r - T_g) \tag{3}$$

The temperature dependence of shift factor for PA6GF30 and PA66GF30 at a reference temperature of 25°C (room temperature) is shown an Fig. 13 As seen there is a very good agreement between the shift factors belonging to PA6 GF30 and PA66 GF30 in the temperature range of 0-150°C. Below 0°C the difference increases drastically as the temperature decreases. In this temperature range, the shift factors for PA6 GF30 are doubtful because the temperature range studied was narrower in [1] than in [2]. Additionatly, the results for PA66 GF30 seen much more realistic in this temperature range. The same is valid for temperatures above 150°C, because the highest temperature an the DMA investigation of [1] was 100°C. On the contrary, in [2], the highest temperature was 200°C. Despite these discrepancies, generally it can be concluded that the temperature dependence of shift factors for PA6 GF30 and PA66 GF30 is very similar. It must be mentioned that below Tg the temperature dependency of PA6 can be described more accurately by the Arrhenius equation. According to this the application of WLF equation in this temperature range is an approximation.

By using the WLF parameters denoted as PA6 GF30 in Fig. 13 the master curve of Ultramid can be estimated from Campus data depicted in Fig. 12a. The result of such a computation i.e. the estimated storage modulus master curve of Ultramid for dry and conditioned state is shown in Fig. 14. It must

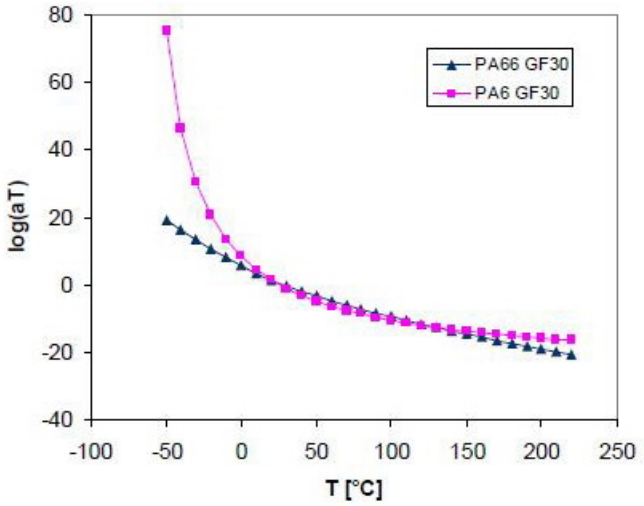

Fig. 13. Temperature dependence of the shift factor (a_T) in case of PA6GF30 ($C_1 = 25$, $C_2 = 100$°C) and PA66GF30 ($C_1 = 74.4$, $C_2 = 502.3$°C for $T > o_r$, and $C_1 = 100$, $C_2 = 468$°C for $T < T_r$) at $T_r = 25$°C. WLF parameters were computed from those of [1] and [2] by Eq. 2 Eq. 3

be mentioned that, as a first approach, the same WLF parameters were used for both the dry and conditioned states. The authors are fully aware that it is a great simplification. The only reason why it is needed is the lack of own DMA measurtments.

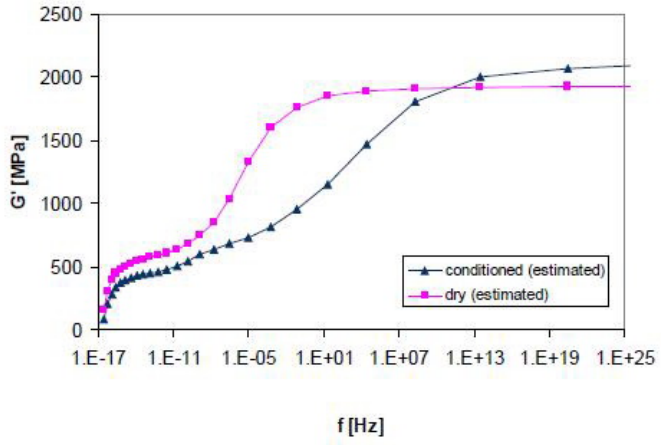

Fig. 14. Estimated (shear) storage modulus master curves of Ultramid at room temperature ($T = 25$°C). These curves were constructed by WLF parameters of $C_1 = 25$, $C_2 = 100$°C.

4.2 Material model

As it was concluded above Utramid exhibits viscoelastic/viscoplastic material behavior. In this study, the viscoelastic/viscoplastic material behavior is modelled by a complex spring-dashpot model. Such a phenomenological modeling approach does not take into consideration the real molecular structure of the material but it may be able to model accurately the macroscopic material response. At the construction ot the viscoplastic material model authors follow the modelling approach of [6]. The key characteristic of this approach is the addition of stresses corresponding to viscoelastic and elastic-plastic constutive model components.

As a first step a viscoelastic model (40-term generalized Maxwels model) is developed to describe the estimated storage modulus master curve of Ultramid (see Fig. 14). Then it is modified to take into consideration the rate independent plasticity. The viscoelastic model used consists of linear springs and deshpots. In case of linear spring, the modulus is constant while the stress-strain relationship is linear. Contrary to this, in case of linear dashpot, the stress-strain rate relationship is linear while their ratio, the viscosity, is constant (stress or strain rate independent viscosity). The generalized Maxwell-model consists of several Maxwell-elements (a linear spring and daspot in series) in parallel and a linear spring connected parallel to the Maxwell elements (see Fig. 15a). It is woth noting that there seems to be no consensus regarding the precise name of the viscoelastic material model used. In FE softwares, research papers dealing with FE modelling and many papers investigating the viscoelastic response of polymers or elastomers (for example in [6]) the material model seen in Fig. 15a is termed as generalized Maxwell-model. However, there are authors who term it as generalized standard-solid model, Weichert-model, or Zener-model. In the present paper, we use the term generalized Maxwell-model. The stress in the generalized Maxwell-model is the sum of stresses in the Maxwell-elements and in the spring. For more detail on the 1-term generalized Maxwell-model (standard solid model) see [11]. As the storage modulus master curve of Ultramid covers more than fourty orders of magnitude in frequency 40-term generalized Maxwell-models were constructed from a fit to storage modulus master curves. The curve fitting i.e. the parameter identification was carried out by the software ViscoData [12]for both the dry and conditioned Ultramid. The comparison of estimated measurement data and constitutive model prediction is shown in Fig. 16. As seen the agreement in very good for both the dry and conditioned states. It is worth noting that the generalized Maxwell-model (see Fig. 15a) is non capable of exhibiting permanent deformation when subjected to a load cycle. Due to this a minor modification is needed in the material model to take into consideration the plastic deformation (see [6]).

In case of n-term viscoelastic generalized Maxwell-model the relaxation modulus can be specified as

$$E(t) = E_0[1 - \sum_{i=1}^{n} ei \times (1 - e^{\frac{-t}{\tau_1}})] = E_\infty + \sum_{i=1}^{n} E_i \times e^{\frac{-t}{\tau_i}} \quad (4)$$

where E_0 is the glassy modulus ($E_0 = E_\infty + \sum_{i=1}^{n} E_i$), τ_i is the ith relaxation time ($\tau_i = \frac{\eta_i}{E_i}$), and e_i is the ith non-dimensional energy parameter ($e_i = \frac{E_i}{E_0}$). Furthermore we can write.

$$\sum_{i=1}^{n} e_i + \frac{E_\infty}{E_0} = 1 \quad (5)$$

In case of dynamic load the frequency dependent storage modulus of the n-term generalized Maxwell-model can be written as

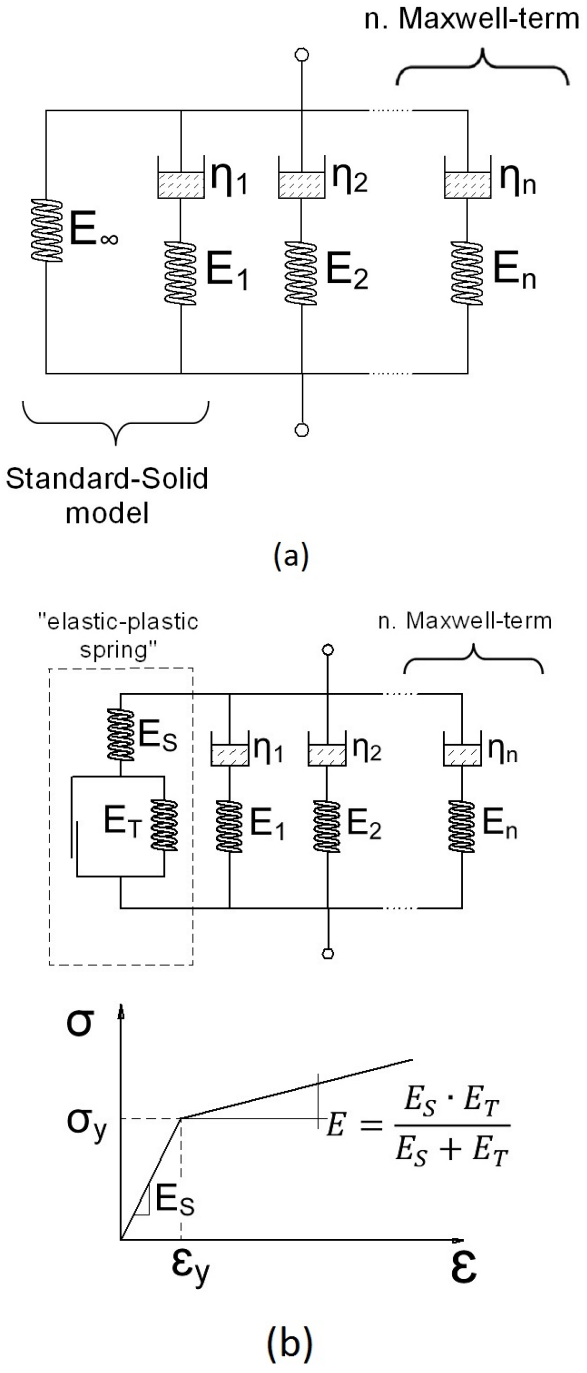

Fig. 15. Schematic representation ta the (t) viscoelastic (generalized Maxwell-model) and (b) viscoplastic material model (E_∞-relaxed modulus, E_i-modulus of the ith spring, η_i-viscosity of the ith dashpot, n- number of Maxwell terms, E_S, E_T- moduli of "elastic-plastic spring", σ_y-yield strength, ϵ_y-yield strain). The mechanical behavior of the "elastic-plastic spring" is shown in the stress-strain diagram.

$$E'(f) = E_0[1 - \sum_{i=1}^{n} e_i] + E_0 \sum_{i=1}^{n} \frac{e_i \tau_i^2 (2 \cdot \pi f)^2}{1\tau_i^2 \, (2 \cdot \pi f)^2} \qquad (6)$$

where f [Hz] is the excitation frequency. Eq. 4 Eq. 5 Eq. 6 can be found in many literatures, among others, in [12] or [13].

According to [6] the generalization of 40-term Maxwell-model to viscoplasticity is made by replacing the linear spring with an "elastic-plastic spring" (see Fig. 15). For the sake of

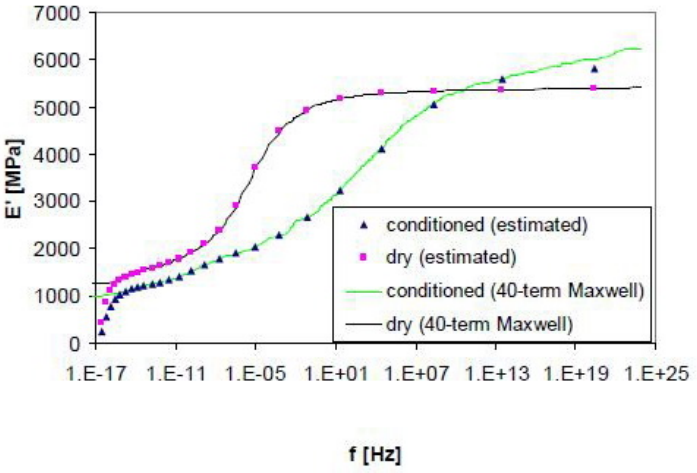

Fig. 16. Comparison of estimated measurement data and constitutive model (40-term generalized Maxwell-model) prediction for both dry and conditioned Ultramid ($T = 25°C$, $Poisson\ ratio = 0.4$).

simplicity the "elastic-elastic spring", in this study, consists of only two linear elastic springs and a "slider element". The "elastic-plastic spring" behaves linearly (with a modulus of E_S) until the element stress does not reach the yield strength (σ_y) because the "slider element" behaves as an idealy rigid element in this range. When the element stress becomes greater than or equal to the yield strengts the "slider element" slides and the spring with modulus E_T starts to work. In other words, the plastic deformation is only active when a yield criterion is met. At and above the yield strength the "elastic-plastic spring" behaves as a linear spring with modulus

$$E = \frac{(E_s \times E_t)}{(E_s + E_t)} \qquad (7)$$

because the two springs (E_S and E_T) are connected in series. As the modulus E_T does not depend on the plastic strain the instantenous modulus E of the "elastic-plastic spring" is plastic strain independent. If one needs a plastic strain dependent "elastic-plastic spring" then the linear spring with modulus E_T has to be replaced by a non-linear spring. In our case, the "elastic-plastic spring" has three parameter (g_S, E_T, σ_y) but, in fact only two parameters must be determined from additional experiments, because E_S is known from the storage modulus master curve ($E_S = E_\infty$). [8] shows clearly that both the yield strength and the subsequent slope of stress increment over the corresponding strain increment are temperature dependent in case of Ultramid. Additionally, it is well known that the yield strength of PA6 GF30 is affected by not only the strain rate but also the moisture content. Generally, the yield strength decreases as the moisture content increases or the strain rate decreases. Unfortunatelly, in [8], there is no experimental data on the temperature, strain rate and moisture content dependency of yield strength and work-hardening slope of Ultramid subjected to compression. In order to overcome this problem and present the capability of the material model authors made the FE simu-

lations with assumed properties. In the viscoplastic FE simulations the Von Mises yield criterion and the isotropic work hardening rule were used. According to the Von Mises yield criterion if the Mises-type equivalent stress reaches the yield strength (σ_y) of "elastic-plastic" spring then plastic strain appears in the boss.

4.3 FE model

FE models have been developed for compression tests to test the capability of viscoelastic and viscoplastic material models introduced in the preceding chapter. In order to realize the complex material model in the FE environment a so called overlay model was used. The basic concept of the overlay model is that the material behavior can be divided into a number of parallel fractions with simple constitutive models and adequate material parameters [10]. The translation of the overlay model in a FE scheme is based on generating a model with several identical overlaid meshes sharing the same nodes. As each FE mesh may have different material behavior it is possible to model even the very complex material responses. Contrary to [10], where the viscoelastic material behavior was neglected, the present work takes into consideration both the time-dependent and time independent effects.

In the present study, the material behaviour of Ultramid was divided into two parts: (a) a rate independent and (b) a rate dependent fraction. The rate independent effects were taken into consideration by an "elastic-plastic" spring (plastic model), while the strain rate dependent effects were modeled by a 40-term generalized Maxwell-model (viscoelastic model). Due to this each FE model consisted of two identical overlaid FE meshes. One of the FE meshes had an elastic-plastic while the other had a viscoelastic material behavior. In other words, one of the meshes was responsible for the time-dependent while the other was repsonsible for time independent effects.

4.4 FE results

Three different axi-symmetric FE models have been developed to model the compression test of Ultramid at room temperature. The first FE model was linear viscoelastic where the material behavior was moleled by a 40-term generalized Maxwell-model (see Fig. 15a). In this case, instead of the overlay model a conventional FE model with single mesh was used. The second FE model was made for verification purposes. The same linear viscoelastic material behavior was modeled as in the first FE model, but, in this case, with the "overlay model approach". Consequently, the FE model had two overlaping meshes. A 40-term generalized Maxwell-model and a linear elastic material model were assigned to the one and the other FE mesh. The modulus of the linear elastic material model corresponded to the relaxed modulus of Ultramid. In order to eliminate the spring with modulus E_∞ from the generalized Maxwell-model the storage modulus master curve was shifted vertically. The aim of this shift was to obtain a practically zero related modulus. Parameters of the modified 40-term generalized Maxwell-model

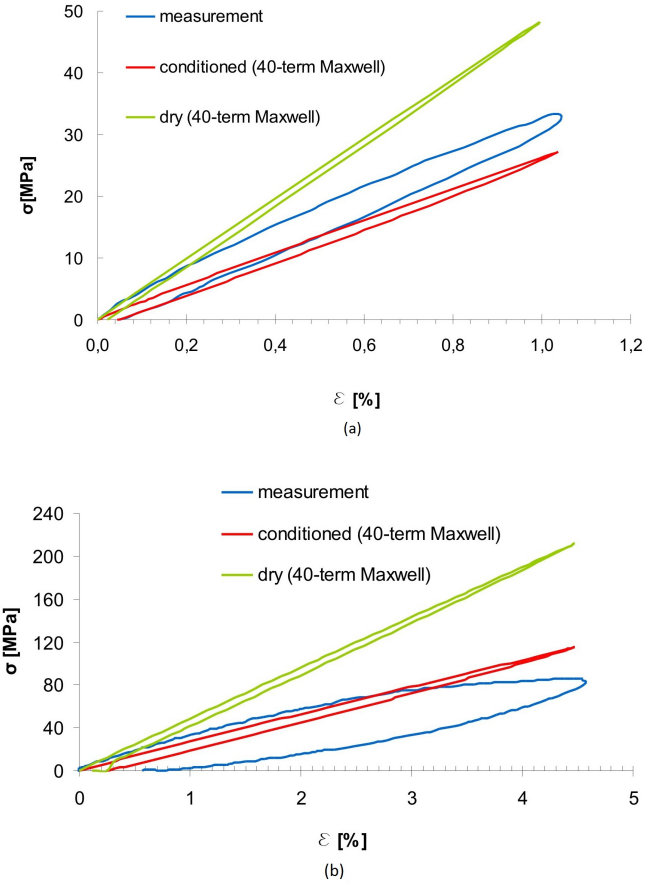

Fig. 17. Comparison of measurement and viscoelastic simulation in case of loading-unloding test:(a) $F = 3$ kN, (b) $F = 8$ kN ($T = 25^oC$).

was then determined from a fit to the vertically shifted master curve. As expected, this vertical shift did not effect the relaxation times of the generalized Maxwell-model. In the viscoelastic overlay model (second FE model), the modified 40-term generalized Maxwell-model was used instead of the original one. Finally, the third FE model was a viscoplastic overlay model where the modified 40-term generalized Maxwell-model and the "elastic-plastic spring" introduced in the preceding chapter was assigned to the one and the other FE mesh.

FE results presented in this chapter were computed by the MSC.Marc software package [13]. Fig. 17 compares the measurement and the viscoelastic prediction in case of compression loading-unloading test. As seen the agreement between measurement and numerical prediction is better for conditioned PA6 GF30 than for dry one. At the same time the accuracy of the predection decreases as the load increases. It can be concluded that the viscoelastic model used is able to predict the material response only at small loads. In order to demonstrate the capability of viscoplastic model proposed authors made simulations with the viscoplastic overlay model too. The results are represented in Fig. 18, Fig. 19.

The measured and computed axial stress-strain response for a loading-unloading test are shown in Fig. 18. As seen there is a good agreement between measurement and numerical prediction. However the measured hysteresis is larger than the pre-

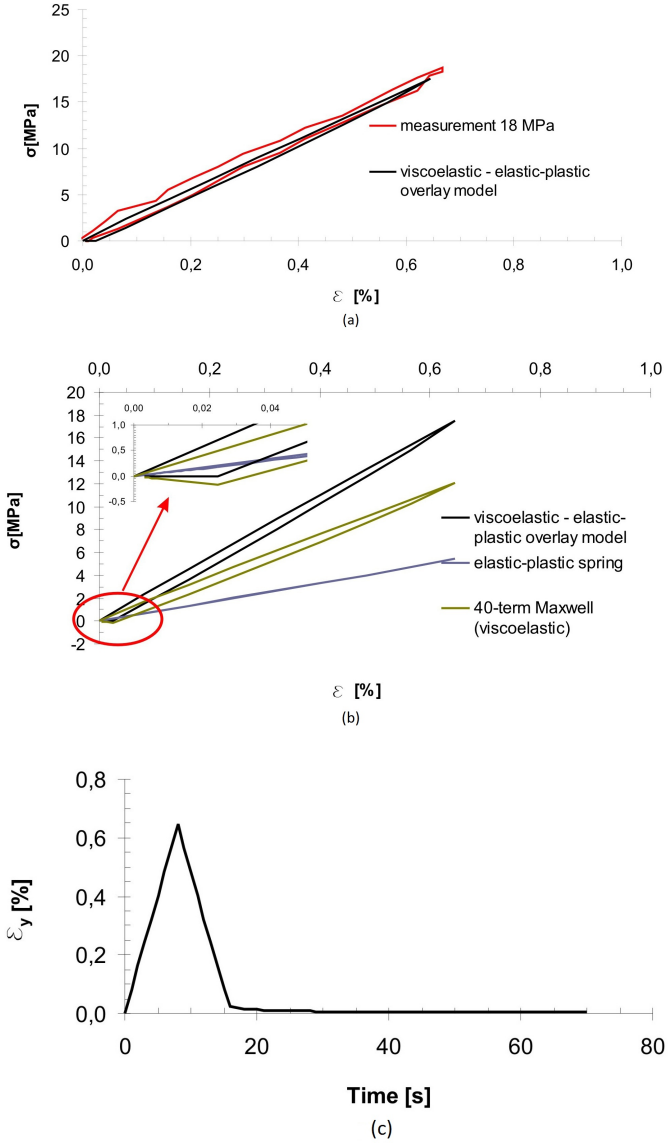

Fig. 18. Computed and measured stress-strain curve, (b) the resulting and the component stress-strain curves, and (c) strain history of the viscoplastic overlay model in case of compression loading-unloading test ($T = 25°C$, conditioned PA6 GF30, $\sigma_y = 20$ MPa, linearly elastic-perfectly plastic ($E_T = 0$ MPa) "elastic-plastic" spring.

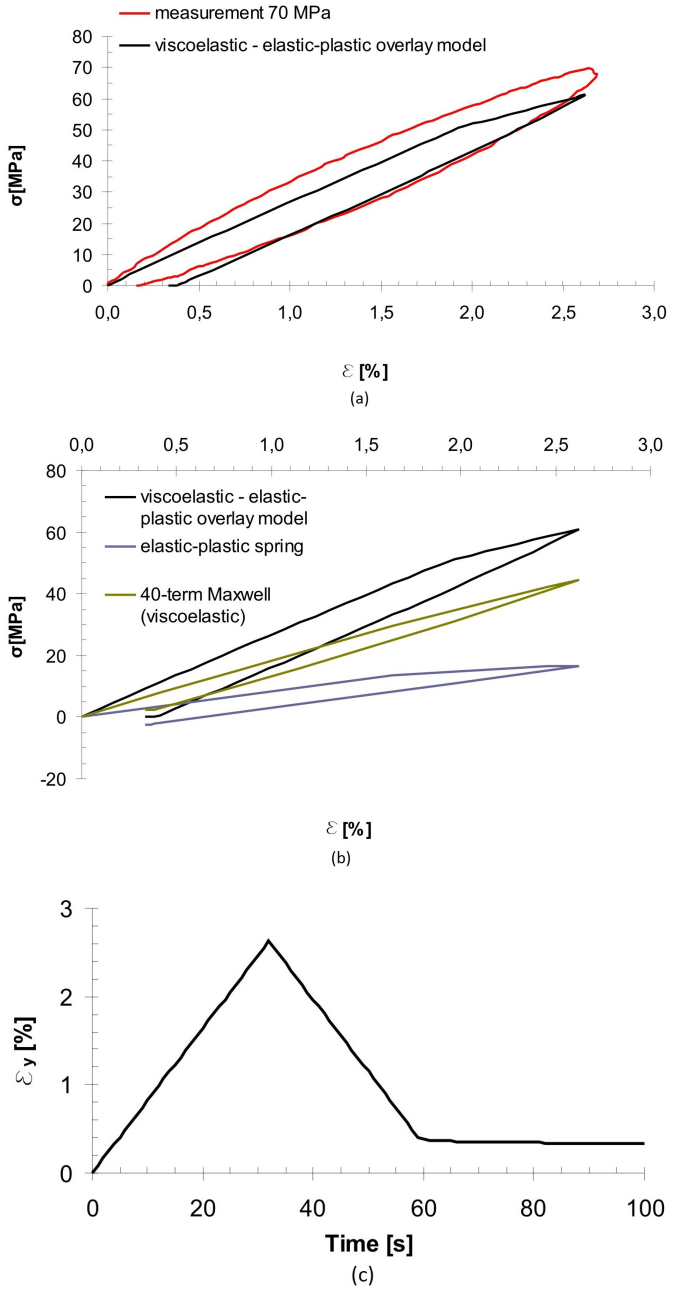

Fig. 19. (a) Computed and measured stress-strain curve, (b) the resulting and the component stress-strain curves, and (c) strain history of the viscoplastic overlay model in case af compression loading-unloading test ($T = 25°C$, conditioned PA6GF30, $\sigma_n = 20$ MPa, linearly elastic-perfectly plastic ($E_T = 0$ MPa) “elastic-plastic” spring).

dicted. It can also be concluded that there is no permanens strain in the prediction because the yield strength of elastic-plastic spring is not reached. The engineering strain history shows (see Fig. 18c) that the strain computed at the end of unloading decreases in fraction of time (strain recovery at zero stress).Fig. 18b shows clearly that the elastic-plastic spring unloads with its initial modulus while the stress decrease in 40-term Maxwell-model decreases is nonlinear. At the end of unloading the resulting stress is zero but the component stresses (viscoelastic and elastic-plastic) are nonzero. The absolute value of component stresses is the same but their sign is different. If the load of the specimen is increated above the yield strength then plastic strains appear (see Fig. 19). In this case the recovery is only partial. As it can be seen, the “elastic-plastic spring” decreased the discrepancy between the simulation and the measurement but the numerical model, even in this case, underestimates the hysteresis. In the present case, due to the estimated material properties of Ultramid it had no sense to fit the material model to our measurements.

5 Summary

First part of this paper is concerned with the mechanical behavior of injection molded PA6 GF30 bosses used to thread-cutting screw joints in compression loading-unloading, cyclic compression loading-unloading and loading-relaxation-unloading-recovery tests. Additionally the fiber orientation and

the strain distribution are also investigated by using scanning electron microscopy and optical grating technique. In the second part, authors present a viscoplastic FE model to simulate the compression loading-unloading tests at room temperature. The material model used can be considered as a generalization of the linear viscoelastic 40-term generalized Maxwell-model to viscoplasticity. According to the overlay method, the FE model has two identical overlaid meshes to model both time-dependent and time independent effects. It is found that the stress-strain response of PA6 GF30 to compression loading-unloading test can not be modeled properly over a certain stress level by a viscoelastic 40-term generalized Maxwell-model. In case when the stress exceeds this stress level the viscoplastic FE model proposed by the authors may be used. The viscoplastic simulation results are realistic and show clearly the flexibility and effectiveness of the modeling approach presented to understand the complex mechanical behavior of PA6 GF30 bosses.

Acknowledgement

The authors express their thanks to Prof. Rainer Renz for enabling them to perform experimental tests in the laboratory of the Department of Mechanical and Process Engineering at University of Kaiserslautern. This work is connected to the scientific program of the "development of quality-oriented and harmonized R+D+I strategy and functional model at BME" phoject. This project is supported by the New Széchenyi Plan (Project ID: TÁMOP-4.2.1/B-09/1/KMR-2010-0002).

References

1 **Mano J F, Viana J C**, *Effects of the strain rate and temperature in stress-strain tests: study of the glass transition ef a polyamide-6"*, Polymer Testing **20** (2001), 937-943.

2 **Stan F, Munteanu A V, Fetecau C**, *Analysis of visco-elastic-plastic behavior of short glass fiber-reinforced polyamide 66 composite (PA66 GF30)*, Materiale Plastice **48/8** (2011), 1-6.

3 **Launay A, Marco Y, Maitournam M H, Raoult I, Szmytka F**, *Cyclic behavior of short glass fiber reinforced polyamide for fatigue life prediction of automotive components"*, Procedia Engineering **2** (2010), 901-910.

4 **Launay A, Maitournam M H, Marmo Y, Raoult I, Szmytka F**, *Cyclic behaviour of short glass fibre reinforced polyamide: Experimental study and constitutive equations*, International Journal of Plasticity **27** (2011), 1267-1293.

5 **Soós E, Renz R**, *Experimental and Numerical Investigations of a Thread–Cutting Screw Joint*, Proceedings of the Third Conference on Mechanical Engineering **2** (2002), 674-678.

6 **Bardenhagen S G, Stout M G, Gray G T**, *Three-dimensional, finite deformation, viscoplastic constitutive models for polymeric materials*, Mechanics of Materials **25** (1997)), 235-253.

7 Conditioning Ultramid moldings, Technical Information, BASF.

8 **CAMPUS®(Computer Aided Material Preselection by Uniform Standards)**, available at `www.campusplastics.com`.

9 **Ferry J D**, *Viscoelaytic properties of polymers*, Wiley (1980).

10 **Gracia L A, Liarte E, Pelegay J L, Calvo B**, *Finite element simulation of the hysteretic behaviour of an industrial rubber. Application to design of rubber components*, Finite Elements in Analysis and Design **46** (2010), 357-368.

11 **Soós E, Goda T**, *Numerical Analysis of Sliding Friction Behavior of Rubber*, Materials Science Forum **537-538** (2007), 615-622.

12 **Herdy M**, *Introductory Theory Manual VistoData and ViscoShift*, IBH-Ingenierbüro (2003), available at `www.vilcodaca.de`.

13 MSC.Marc. Volume A, Theory and User Information, Version 2007R1.